

Flytrap-inspired robot using structurally integrated actuation based on bistability and a developable surface

This content has been downloaded from IOPscience. Please scroll down to see the full text.

2014 Bioinspir. Biomim. 9 036004

(<http://iopscience.iop.org/1748-3190/9/3/036004>)

View [the table of contents for this issue](#), or go to the [journal homepage](#) for more

Download details:

IP Address: 147.46.146.163

This content was downloaded on 12/03/2014 at 01:18

Please note that [terms and conditions apply](#).

Flytrap-inspired robot using structurally integrated actuation based on bistability and a developable surface

Seung-Won Kim¹, Je-Sung Koh¹, Jong-Gu Lee², Junghyun Ryu², Maenghyo Cho² and Kyu-Jin Cho¹

¹ Biorobotics Laboratory, School of Mechanical and Aerospace Engineering, Institute of Advanced Machinery and Design, Seoul National University, 151–744, Seoul, Korea

² Smart Structures & Design Laboratory, School of Mechanical and Aerospace Engineering, Institute of Advanced Machinery and Design, Seoul National University, 151–744, Seoul, Korea

E-mail: kjcho@snu.ac.kr

Received 26 December 2013


Accepted for publication 10 February 2014

Published 11 March 2014

Abstract

The Venus flytrap uses bistability, the structural characteristic of its leaf, to actuate the leaf's rapid closing motion for catching its prey. This paper presents a flytrap-inspired robot and novel actuation mechanism that exploits the structural characteristics of this structure and a developable surface. We focus on the concept of exploiting structural characteristics for actuation. Using shape memory alloy (SMA), the robot actuates artificial leaves made from asymmetrically laminated carbon fiber reinforced prepregs. We exploit two distinct structural characteristics of the leaves. First, the bistability acts as an implicit actuator enabling rapid morphing motion. Second, the developable surface has a kinematic constraint that constrains the curvature of the artificial leaf. Due to this constraint, the curved artificial leaf can be unbent by bending the straight edge orthogonal to the curve. The bending propagates from one edge to the entire surface and eventually generates an overall shape change. The curvature change of the artificial leaf is 18 m^{-1} within 100 ms when closing. Experiments show that these actuation mechanisms facilitate the generation of a rapid and large morphing motion of the flytrap robot by one-way actuation of the SMA actuators at a local position.

Keywords: bioinspiration, soft robotics, flytrap, bistability, structurally integrated actuation

 Online supplementary data available from stacks.iop.org/BB/9/036004/mmedia

(Some figures may appear in colour only in the online journal)

1. Introduction

In nature, many living creatures utilize structurally integrated actuation. One interesting example, which shows a dramatic morphing motion using actuation without any muscle-like element, is an insectivorous plant. The Venus flytrap (*Dionaea muscipula*) catches agile insects by changing the shape of its soft leaf from open to closed within 100 ms. Due to this interesting feature, researchers have investigated the mechanism of the leaf motion [1–6], and developed artificial flytraps that mimic the shape and motion of the flytrap [7–9].

The rapid morphing motion of the leaf results not from a rotation of the leaf through use of a hinge-like structure but from a transformation of the shape—i.e., morphing—using bistability, the structural characteristic of the leaf [4]. The flytrap leaf is a bistable structure that has two stable states resulting from the asymmetric pre-strain field of the leaf. As a result, it has different shapes for each stable state: an almost flat state when the leaf is open and a concave state when the leaf is closed. When the flytrap changes the leaf shape from one stable shape to the other, the flytrap controls only the turgor pressure to adjust the state of the leaf: the state is

related to the shape of the leaf. As the state passes through a critical state between two stable states, a rapid shape transition occurs: this is called snap-through and is a common feature of the bistable structure. Therefore, the actuation procedure of the flytrap is divided into two parts: the triggering actuation by the turgor pressure as the explicit actuation agent and the snap-through actuation by the bistability as the implicit actuation agent. Using bistability, the flytrap needs actuation energy only for the triggering actuation; thus, the flytrap uses vital energy efficiently and produces rapid motion that is hard to obtain from muscle-less systems of *Plantae*.

The motion a flytrap can be implemented with a soft robotics technology, which uses the large deformation of a soft body to create motion. In soft robotics, an important issue is creating the desired motion of a soft-body robot by effective and efficient actuation. Traditional hard robots are made of rigid links and joints, which have a finite number of degrees of freedom (DOF). The motion of such robots is governed by mechanisms based on rigid body kinematics and is generally driven by an explicit actuation agent, such as motors with sensors and controllers [11]. In contrast, soft robots are made of flexible material, and provide several advantages: capability of creating dexterous motion, high adaptability to various environments and multiple functionalities from a single structure [12–15]. Owing to the infinite number of DOF and nonlinearity of the soft structure, however, it is difficult for soft robot design to harness these features effectively.

For soft robots, structurally integrated actuation—an actuation method that utilizes the embedded characteristics of the structure—helps control the infinite DOF effectively and efficiently. For example, the meshworm robot [16] uses the constant-wire-length constraint of the mesh tube to control the size of the tube diameter, which enables the creation of a back-and-forth linear motion, i.e., peristaltic locomotion. Similarly, the soft robotic arm inspired by the octopus [17, 18] also uses the characteristics of the mesh tube to generate dexterous motion. A pneumatic network channel is embedded into the soft robot structure by soft lithography, and the single pneumatic actuation through the channel creates various motions such as bending/unbending [19–22], twisting [22], and elongation [21]. In these examples, the structural characteristics act as a kinematic constraint, which reduces the number of controlling DOF from infinite to a few; the detailed motion trajectory is determined passively. The structural characteristics can also be regarded as an implicit actuation agent: it does not appear on the outside but influences the generation of the motion. The role of structurally integrated actuation is related to the concept of ‘embodied intelligence,’ where the desired motion and function are realized through a novel hardware design that gives the structure intelligent characteristics. Using structurally integrated actuation, a soft robot with a simple control mechanism, and a simple and light structure, can perform functions effectively.

In our previous works [7, 8], we developed the preliminary prototypes of a flytrap robot that show rapid morphing speed and large morphing deformation. The bistability, which is the source of the structurally integrated actuation, was attained

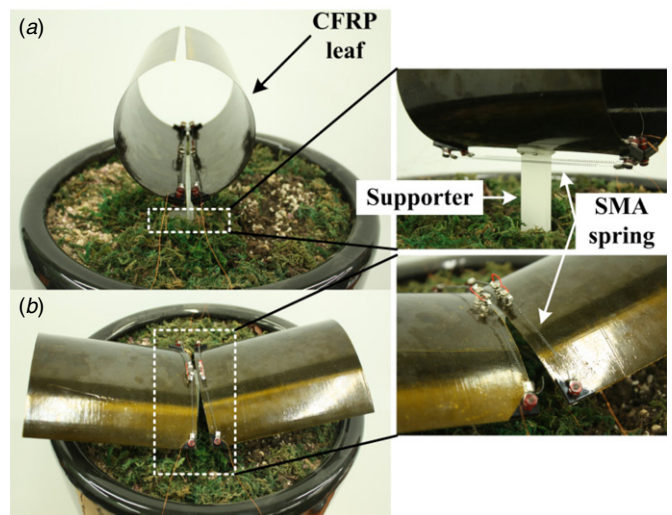


Figure 1. Bio-inspired flytrap robot with (a) CFRP leaves closed and (b) the leaves open. Two CFRP leaves are fixed on the supporter. Both ends of SMA springs are attached at two corner of the CFRP leaf.

by using an asymmetrically laminated carbon fiber reinforced prepreg (CFRP) structure that acts as the artificial leaves of the flytrap robot. The actuator of the robot is a shape memory alloy (SMA) coil spring actuator that only works for the triggering actuation to induce the snap-through.

In this paper, we introduce a new triggering actuation for opening the artificial leaf of the new flytrap robot, as shown in figure 1. To mimic the shape of the flytrap leaf, the artificial leaf has two different radii of curvature in two stable states. In particular, it has a large curvature in the closed state. For opening, the previous triggering actuation of the shape with the large curvature required a bulky actuation part [8] and induced a local buckling problem [10]. The new triggering actuation overcomes these limitations.

The new triggering actuation for opening is activated by a simple one-way input of the actuator, which induces snap-through actuation of the artificial leaf. It generates local bending deformation at one straight edge of the curved bistable CFRP structure and propagates the deformation until the snap-through action occurs; we call this bend-propagating actuation (BPA). The shape of the artificial leaf is successfully changed from a semicircle to flat by using the BPA. The structurally integrated actuation using the bistable CFRP structure generates the rapid closing motion of the flytrap robot; the closing time of 100 ms is the same as that of the flytrap.

The rest of the paper is organized as follows. In section 2, basic information on the bistable CFRP laminate is presented to clarify the principle of bistability and the features of the robot. Then, in section 3, BPA is explained, including the SMA coil spring actuator arrangement. In section 4, the manufacturing processes of the bistable CFRP laminate as an artificial flytrap leaf and the SMA coil spring as an actuator are presented. In section 5, the experiment on the shape transition and a loading test for the bistable CFRP laminate by BPA, as well as the test of the SMA spring actuation, are described. The experiment results are compared with those of a numerical simulation by the finite element method, and

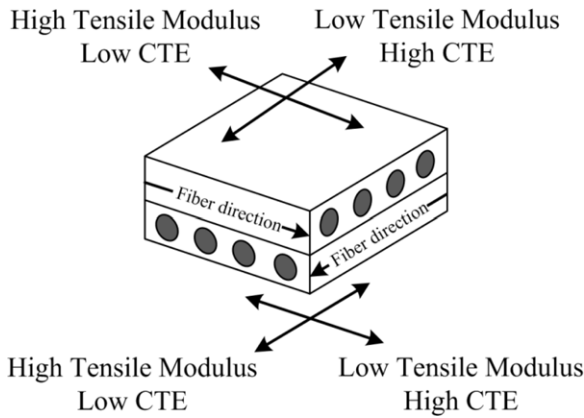


Figure 2. Different material characteristics according to the fiber direction. (a) Lateral side view and (b) frontal side view of the CFRP ply. CF refers to carbon fiber. (c) Directional thermomechanical characteristics of the cross-ply CFRP laminate. CTE refers to the coefficient of thermal expansion.

video data are analyzed by image processing (available from stacks.iop.org/BB/9/036004/mmedia). Finally, in section 6, the closing and opening motions and capturing performance of the flytrap robot are performed, analyzed and discussed.

2. Brief summary of asymmetrically laminated CFRP and its bistability

The bistability of the asymmetric CFRP laminate is based on the directional characteristics of CFRP ply (see figure 2). A single CFRP ply consists of unidirectional carbon fibers and epoxy resin. The tensile modulus of the CFRP ply is about ten times higher in the carbon fiber’s axial direction than in the fiber’s lateral direction because the modulus in the lateral direction depends only on the adhesion of the resin matrix between fibers. Thermal expansion of the CFRP also has directional features. The coefficient of thermal expansion (CTE) in the lateral direction is about one hundred times that in the fiber’s axial direction.

Owing to the directionality of the CFRP ply, the CFRP laminate can form a bistable structure through the asymmetrical stacking of the plies. The asymmetric layering causes a difference in mechanical properties between the layers (see figure 2(c)). The tensile modulus of one layer is larger than that of the other layer, while the CTE of one layer is smaller than that of the other layer in a certain direction. The difference from the asymmetric layering induces a residual thermal stress (RTS) on the laminate after the manufacturing process. The RTS develops a pre-strained field, which forms two stable shapes in the laminate at room temperature; as a result, bistability is created. Owing to the snap-through action by the bistability, changes from one stable shape to the other are very fast. The two stable shapes are cylindrical; the axes of curvature are orthogonal to each other if the plies are stacked perpendicularly. Figure 3 describes the detailed process of how this cross-ply CFRP laminate creates bistability.

Interestingly, the cross-ply CFRP laminate has two common features with the flytrap leaf: an orthogonal curvature shape and the snap-through action, both of which originate

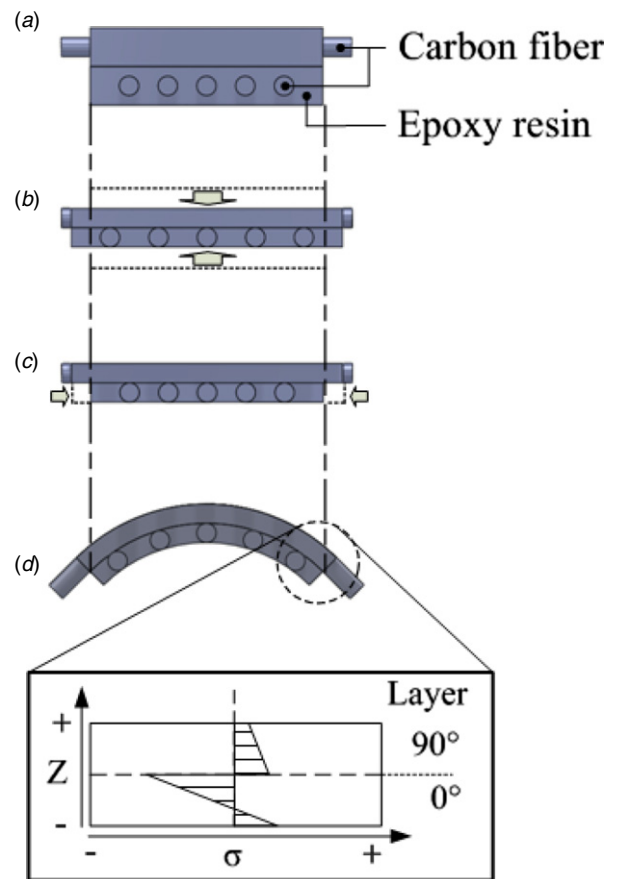


Figure 3. (a) Cross-ply CFRP laminate at room temperature before curing. (b) The laminate is pressed and expanded under high temperature and pressure during curing. (c) After curing, owing to the mismatched thermomechanical characteristics of the upper and lower layers, the expanded epoxy resin asymmetrically shrinks as it is cooled to room temperature. (d) Owing to the boundary condition, the final configuration of the cross-ply CFRP laminate is curved after curing is finished at room temperature. The enlarged part of the dashed circle area in (d) shows the stress distribution of the boundary. Z is the thickness-through height for which the reference is the mid-plane of the laminate. σ is the normal stress of the CFRP layer. A positive stress means compression, and a negative one means tension. Note that the illustration is exaggerated to facilitate understanding.

from the bistability. Based on these common features, we can employ the cross-ply CFRP laminate as an artificial leaf of the flytrap robot that can be shut rapidly by using the snap-through action.

3. Design

In this section, the design concept of the new flytrap robot and detailed design issues are discussed. The artificial leaf of the flytrap robot is a cross-ply bistable CFRP structure, and the triggering actuator is an SMA spring actuator. The shape of the artificial leaf mimics that of the flytrap leaf, which has different radii of curvature in two stable states. The curvature of the bistable CFRP in one stable state can be adjusted using the curved tool-plate as a mold. To close and open the artificial leaf, actuation has to generate a curvature change. The curvature change of the bistable CFRP structure

exploits the characteristic of a developable surface in that only one nonzero curvature axis exists at any point on the surface. Owing to the different curvatures of the artificial leaf in the two stable states, the flytrap robot uses two different types of actuation to change the curvature: a common unbending actuation to close the leaf with the small curvature and a BPA to open the leaf with the large curvature.

3.1. Curvature adjustment of the bistable CFRP leaf

The leaf of the flytrap has different curvatures at different stable shapes. When the leaf is open, its shape is almost flat; when the leaf is closed, the shape is domelike. This asymmetric shape of the flytrap leaf is the desired shape of the artificial leaf of the flytrap robot. Normally, the curvatures of the two stable states of a square-shaped CFRP laminate are identical when it is cured on a flat surface. Therefore, a method for adjusting the curvature of the bistable CFRP laminate is needed.

According to previous studies [23, 24], the curvature can be adjusted by varying the geometric parameters of the CFRP laminate, such as the thickness ratio and stacking order except side length. The side length of the CFRP laminate determines not the curvature but the existence of bistability: over a critical side length of the CFRP laminate, the CFRP laminate has bistability and its curvature quickly converges to a constant value. However, such adjustment methods are not suitable for inducing the major change in curvature from flat to semicircle. The CFRP layer thickness and the region where bistability exists limit the adjustable thickness ratio, and the change of curvature is small. Adjusting stacking order method requires more than three CFRP layers, and this increases the total thickness of the laminate, which produces smaller curvature than two-layered bistable CFRP laminate.

In order to adjust the curvature by a large amount, we use a curved tool-plate as a curing mold. We developed a constitutive model to analyze the effect of using the curved mold with the laminate and then verified the result with an experiment in the previous study [25]. Based on numerical analysis with the model, the curvature variation of the laminate depending on the curvature of the tool-plate can be plotted, as shown in figure 4. The graph shows that the tool-plate curvature affects one stable curvature of the laminate but not the other. Based on the results, we used a tool-plate with an -8.33 m^{-1} curvature to produce the desired configurations: an almost flat shape and a large curved shape. We did not choose the -10 m^{-1} tool-plate because the laminate cured on a tool-plate with a large negative curvature has a very flat shape as one stable shape, so the bistability is very weak.

3.2. Triggering actuation

The structurally integrated actuation of the bistable CFRP structure is divided into two parts: triggering actuation and snap-through actuation. The triggering actuation unbends the curved structure until the snap-through actuation occurs. Thus, the design of the triggering actuation, especially the unbending actuation, is the key issue for actuation of the flytrap robot. In this section, the features and limitations of the previous common unbending actuation are explained.

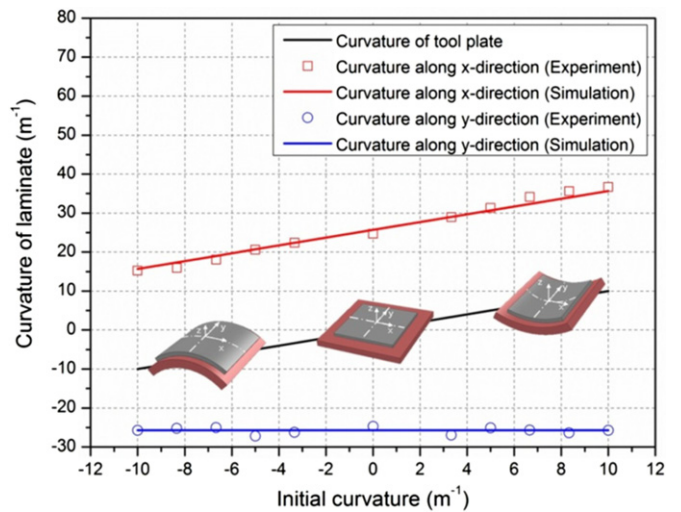


Figure 4. Distribution of the curvature of CFRP laminates with different initial curvatures during manufacturing [25]. The upper red line changes along the curvature of the jig plate (middle black line), whereas the lower blue line remains unchanged. The solid line shows the numerical result, and the hollow circles and squares show the experimental result. The variation in the experimental result is due to environmental effects, such as moisture absorption and relaxation of the resin over time.

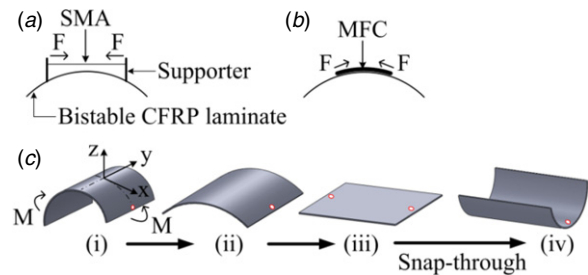


Figure 5. Actuator arrangements of common unbending actuation with (a) SMA wire or SMA spring actuator and (b) MFC actuator. (c) Process of common unbending actuation. The red circle in (c) indicates the actuation point.

Then, the concept of using the structural characteristics to improve the unbending actuation is briefly summarized as a characteristic of a developable surface. Finally, the BPA using the developable surface characteristic is introduced.

3.2.1. Common unbending actuation. Previous investigations of morphing structures and smart structures using the bistable CFRP structure introduced intuitive unbending actuation with various actuators. Dano *et al* [26], Schultz *et al* [27] and Hufenbach *et al* [23] used an SMA wire actuator and macro fiber composites (MFC) actuator (which is a kind of piezoceramic actuator), respectively. Kim *et al* [28] used an SMA wire and an MFC actuator together for repeatable antagonistic actuation. In the previous prototypes of the flytrap robot [7, 8], the SMA coil spring was used. As shown in figures 5(a) and (b), the common feature of these unbending actuations is that the actuator is located on the curve, which is the circumference of the structure. The actuator applies

the force or moment to the structure along the curve and unbends the curved structure until it becomes flat, as shown in figure 5(c), and the snap-through actuation occurs. We call such actuation the common unbending actuation.

The curvature of the artificial leaf of the flytrap robot in one stable state is much larger than that in the previous investigations [7, 8, 23, 26–28]. If the curved structure has a large curvature, common unbending actuation using SMA wire, SMA spring and MFC actuators has several limitations. When using SMA wire and SMA spring, unbending is performed by tendon-driven actuation (see figure 5(a)). Such actuation generates a bending moment at two actuation points connected to the SMA actuator. If the curvature of the structure is small, the bending moment is sufficient to completely unbend the structure. However, if the curvature is large, this actuation only unbends a local part of the curve, and the rest of the curve remains unchanged. In addition, the actuation can create local buckling, and the structure would be distorted [10]. To avoid this problem, this unbending actuation requires a large supporter as a moment arm, or many long supporters. However, the supporters make the design of the structure complicated and bulky. The bending deformation of the MFC actuator is very small. If we attach several MFC actuators on the surface along the curved line of the structure, the bending deformation increases slightly. However, attaching the actuator on the surface reduces the original curvature of the structure because the bending stiffness of the attached MFC actuator affects the bending stiffness of the whole structure. As a result, the common unbending actuation is inapplicable to the large curved shape of the artificial leaf. To overcome these limitations, we exploited the structural characteristic of the bistable CFRP structure—i.e., the feature of a developable surface. This characteristic allows BPA to create the desired unbending motion, even though the direction of actuation is perpendicular to that of the motion.

3.2.2. Developable surface characteristic of the bistable CFRP structure. The curvature tensor at a point of the thin shell in a stable state has two principal curvatures: maximum and minimum curvatures. According to Gauss' theorema egregium [29], the product of two principal curvatures at this point is a Gaussian curvature whose sign can be used to characterize the surface: positive implies that the surface is domelike, negative implies that the surface is a saddle, and zero implies that the surface is flat or rolled. The surface with a zero Gaussian curvature is a developable surface. If a developable surface changes to a non-developable surface, the surface should be stretchable or compressible in plane. If a surface such as a metal sheet, stiff paper or CFRP is hard to stretch or compress in plane, the Gaussian curvature of the surface is zero. This means that the surface should have at least one zero principal curvature. It allows only a rolled shape with a single curvature axis or a flat shape—i.e., a developable surface.

The cross-ply bistable CFRP structure has a cylindrical shape in each stable state, as shown in figures 6(a) and (b). The bistable CFRP structure is neither stretchable nor compressible, thus it has the same characteristic as that of a developable surface. Therefore, one of the principal axes must

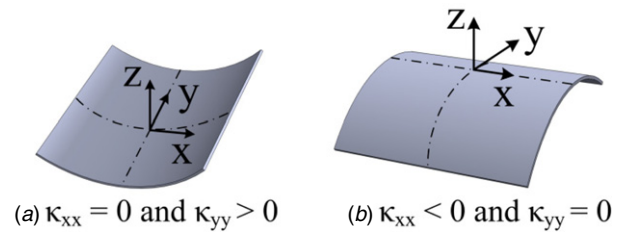


Figure 6. Reference coordinates of the bistable CFRP with principal curvature directions and signs. (a) is one stable shape and (b) is the other stable shape.

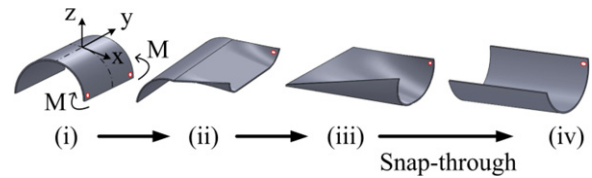


Figure 7. Process of bend-propagating actuation. The red solid circle represents an actuation point. M indicates the bending moment. At the moment between (iii) and (iv) snap-through action occurs. The red circle indicates the actuation point.

have zero curvature, while the other has a nonzero curvature. This implies that the bistable CFRP structure needs unbending actuation to change the nonzero principal curvature κ_{yy} to zero in order to snap-through from one stable state (figure 6(a)) to the other (figure 6(b)).

3.2.3. BPA. Although the initial and final shapes of the CFRP are the same as those in common unbending actuation, the BPA shows a different deformation process; paradoxically, the BPA uses bending to induce the unbending motion.

Common unbending actuation applies the force along the curve, which induced the unbending of the curved structure. In contrast, the BPA applies the force perpendicular to the curve, as shown in figure 8. As shown in figure 7(i), the actuation points (red circle dots in the figure) are located near the straight edge ($\kappa_{xx} = 0$). When the actuator applies a force or moment to the actuation points, the straight edge starts to bend, and this bending propagates along the curve ($\kappa_{yy} < 0$) on the x -axis. Owing to the characteristic of the developable surface, which allows only one zero principal curvature at any point on the surface, the two principal curvatures at every point on the surface flip sign: the original straight line ($\kappa_{xx} = 0$) on the surface becomes a new curve ($\kappa_{xx} > 0$), while the original curve ($\kappa_{yy} < 0$) becomes a new straight line ($\kappa_{yy} = 0$). This progresses until the original curve is removed, and snap-through occurs. After snap-through, the new curve becomes the circumference of a cylindrical shape in the other stable state, and the structure changes its shape from one stable shape to the other. This actuation propagates the bending deformation; thus, we call the novel unbending actuation BPA.

3.3. Design concept of flytrap robot

The flytrap robot comprises three components, as shown in figure 8: two bistable CFRP leaves, two SMA coil springs at

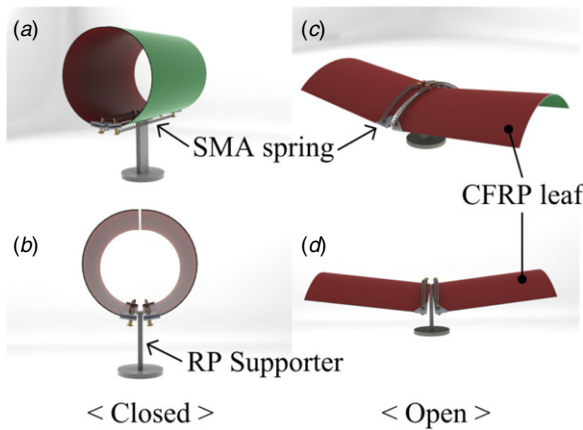


Figure 8. Conceptual design of the flytrap robot. (a) and (b) show the robot closed. (c) and (d) show the robot open. To distinguish the upper and lower surfaces on the CFRP leaf, the upper and lower sides are colored red and green, respectively.

each leaf and a supporter that holds the leaf. The center part of the straight edge of the artificial leaf with a large curvature is mounted on top of the supporter, which acts like the midrib of the flytrap, and two mounted leaves are opposite each other. Typically, the SMA wire and MFC actuator of the previous common unbending actuation generate a small deformation. Instead of using these actuators, we chose the SMA coil spring actuator for its advantages: a large stroke and high power density, which is the ratio of the generating force to the weight of the actuator [30–33]. For the different radii of curvature of the artificial leaf, we used different types of actuation with the curvature. When the leaf has a small curvature in the open state, common unbending actuation is appropriate for the closing motion. When the leaf has a large curvature in the closed state, BPA is appropriate for the opening motion. Based on the actuation direction of each actuation type, two SMA spring actuators are located on the surface of the leaf near the supporter, but one is on the upper side and the other is on the lower side. This actuator arrangement concentrates actuators at one end of the surface of the artificial leaf. This allows for most of the surface of the artificial leaf to be clear of the actuator and additional matter, thus enabling a simple structure of the robot. Both ends of the SMA spring actuator are connected to bolts that are mounted at the corners of the leaf. The supporter was fabricated by a rapid prototyping process. A fine enamel-coated wire is used as an electrical power line to activate the SMA spring actuator. When the SMA spring is activated by electric heating, the actuator pulls the corners, and the bending moment is applied. Then, the snap-through action is induced, and shape transition of the structure is achieved.

4. Manufacturing

4.1. Different initial curvature CFRP laminate

In order to make the artificial leaf with asymmetric curvature, a cross-ply laminate is placed on a curved tool-plate mold made by bending a heat-treated steel plate to form the desired curvature. Table 1 lists the material properties of CU 0503 type CFRP (Hankuk Carbon Co., Ltd), which was used in this

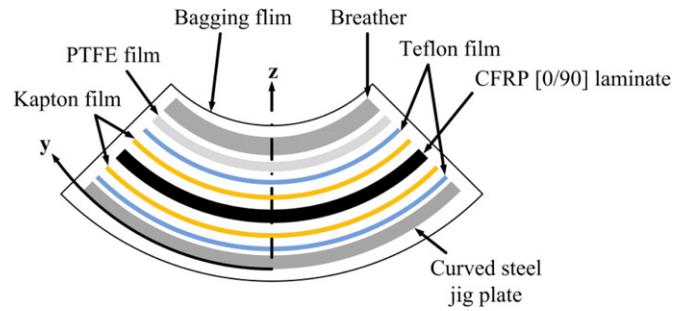


Figure 9. Stack-up arrangements of the materials in the curing package and an illustration of curing processing. The x-axis is in the inward direction into the paper.

Table 1. CFRP material properties^a.

Quantity	Unit	
Axial tensile modulus, E_1	GPa	160
Transversal tensile modulus, E_2	GPa	12
Shear modulus, G_{12}	GPa	8
Poisson's ratio, ν_{12}		0.3
Density	g cm^{-3}	1.8
Thickness	mm	0.092
Axial CTE ^b , α_1	$^{\circ}\text{C}^{-1}$	0.19×10^{-6}
Transversal CTE ^b , α_2	$^{\circ}\text{C}^{-1}$	32.0×10^{-6}
Temperature change, ΔT^c	$^{\circ}\text{C}$	-145

^a These data are from Hankuk Carbon Co., Ltd.

^b CTE is the coefficient of thermal expansion.

^c Temperature change, ΔT , is the difference between room temperature and the curing temperature.

study. For the stacking order of the cross-ply laminate, the first ply is aligned with its fiber direction along the curvature axis of the tool-plate, and the second ply is aligned with its fiber direction perpendicular to the curvature axis of the tool-plate. The laminate is trimmed to a square with side lengths of 150 mm before the curing. The cross-ply laminate is covered on both sides with 25 μm thick Kapton film to prevent electric conduction on the CFRP surface by actuation of the SMA actuator. The laminate covered with Kapton film is sandwiched between two release films to prevent the laminate from sticking to the mold after curing. The laminate is placed on the mold, and a thick PTFE sheet film is laid on top of the laminate to produce a smooth outer surface. The laminate package is covered with a breather. Finally, a bagging film is wrapped around all of the materials, including the mold, and the package is sealed with a sealant tape to maintain a vacuum inside the bag. Figure 9 shows the material stack-up arrangement. In this study, the curing temperature was increased from room temperature of 25–170 $^{\circ}\text{C}$ for a curing time of two hours. The curing pressure was kept at one atm by an external vacuum pump during the curing cycle.

4.2. SMA coil spring

This study referred to several investigations that presented the basic manufacturing method of an SMA coil spring actuator [30, 33]. Before the heat-annealing process, to induce shape memory, the SMA wire is wound to a steel rod by an electric

Table 2. Sample SMA spring properties^a.

Quantity	Unit	
Wire diameter	mm	0.254
Spring mean diameter	mm	1.254
Spring index		4.937
Austenite starting temperature	°C	70
Coil number		20
Initial length	mm	5
Actuation stroke	mm	25

^a SMA wire is from Dynalloy Inc.

hand drill device and fixed by clamping with bolts and nuts. The wound SMA wire is then placed in a furnace and annealed at 300 °C for an hour. After the heating process, the wound SMA wire is cooled naturally, and a coil spring shape is maintained. Table 2 provides the geometric information of the sample SMA spring. Based on the sample spring, the initial length of the SMA spring actuator used in the robot is adjusted from the stroke of the sample. The manufactured SMA coil spring has different actuation characteristics from the original SMA wire. Although the SMA coil spring can generate approximately 3.5 N, which is one-third of the force generated from the SMA wire, the spring has approximately 500% of the actuation stroke of the wire. The sample SMA spring had 20 coils, and its stiffness was approximately 0.15 N mm⁻¹.

5. Experiments and results

This section shows various experiments and results to investigate characteristics of flytrap robot. The first subsection about snap-through action by BPA includes a load profile of bistable CFRP leaf by BPA and the result is compared with the numerical simulation result by ABAQUS and snapshot figures of shape transition. This shows that BPA generates the propagation of bending moment and snap-through action to the bistable CFRP leaf successfully. The second subsection deals with the actuation of SMA spring actuator and its operating condition for the appropriate actuation of flytrap robot. The third and fourth subsections show the rapid locomotion and capturing performance of flytrap robot.

5.1. Snap-through action by BPA

The tensile experiment shown in figure 10 was designed to obtain a load profile of the snap-through action by BPA. Near one straight edge of the CFRP laminate, acrylic triangle washers were bolted to the corners, giving a total moment arm length of 8 mm. At the center of the edge, a rectangular washer is mounted to set a same constraint applied by the leaf mount in the robot. A wire was connected from one bolt to the other, passed through a slit attached to the post, and connected to a load cell with a linear motor. The linear motor applied force to the wire, creating a bending moment at the corner points. Propagation of the bending moment induced snap-through at which point linear actuation ceased. The load cell measured force applied by the linear motor, and the displacement of the

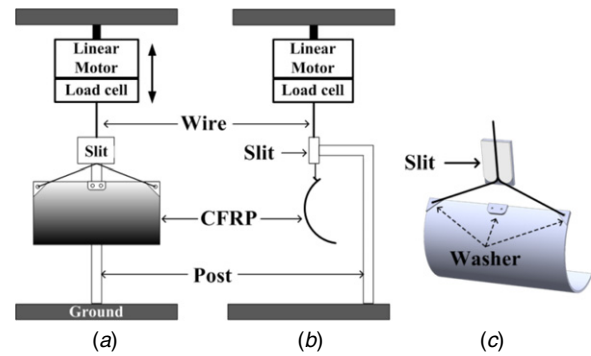


Figure 10. Experimental setup of the BPA test at (a) frontal view and (b) side view. (c) Expanded view of the connection between the CFRP and wire through the slit.

two corners was calculated from linear motor displacement sensor data.

Tests were performed for two transitions: from the small curved shape to the large curved shape, which is equivalent to closing; and from the large curved shape to the small curved shape, which is equivalent to opening. Each case was tested three times for consistency. The small curved shape required a smaller displacement and force than did the large curved shape for snap-through to occur. The experimental results were compared with numerical simulation results from ABAQUS.

The ABAQUS models consisted of the bistable composite and the three washers, illustrated in figure 10(c). The 4-node doubly curved thin shell element (S4) and the linear quadrilateral element (R3D4) were used to generate the mesh, respectively, in the bistable composite and the washer parts. The mesh density of the bistable composite part was chosen as 30 × 30(900 elements, element size of 5 mm) in consideration of convergence properties and computation time. The washer was represented by choosing 28 elements with element size of 4–5 mm, assuming perfect bonding between the surface of the bistable composite and the washer part. The interaction condition was set as a perfect bonding condition that the element of the washer and that of the composite is directly connected.

Finite-element analysis of the snap-through is divided into two main processes: curing and loading processes. For both processes, the bistable composite is fixed at the center washer to remove rigid body rotation and translation, while the corners of the bistable composite move freely during the curing process, but are constrained to move along the tensile direction of the wire during the loading process. The bistable composite is an anisotropic plate body; i.e., materials for which the constitutive behavior is direction-dependent and a plane stress state. For the bistable composite, the material property is based on table 1.

The ABAQUS simulation result is in figure 11(c), and it shows good agreement with the experimental result. The stress of the bistable CFRP structure due to the bending moment increases from both corners at first, and the stress wave propagates to the opposite direction gradually. Based on the snap-shots of experiment and simulation results, each point of the load profile with italic numbers in figure 11(a) is explained in detail:

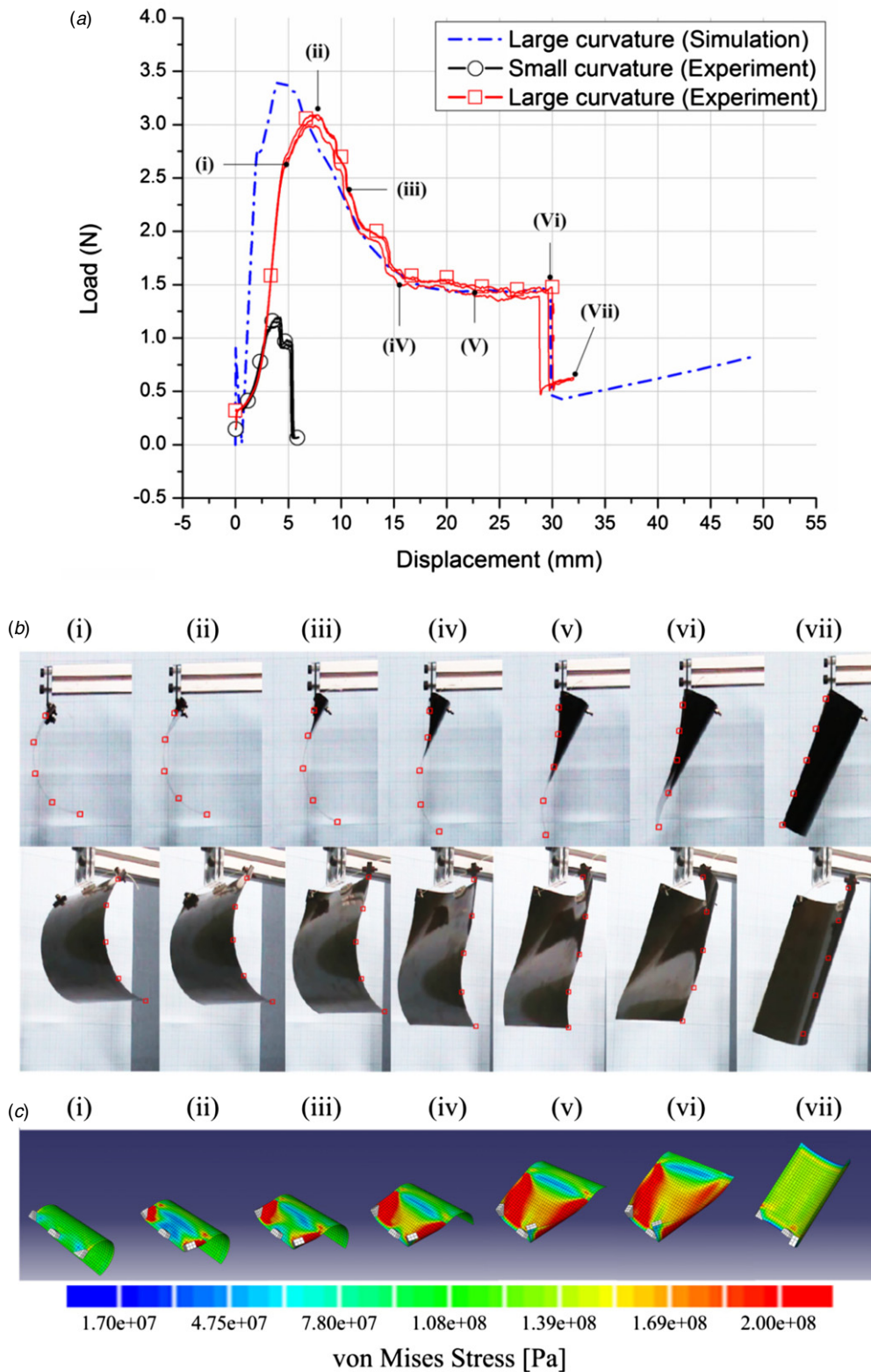


Figure 11. (a) Experimental and simulation results of load profile of the CFRP laminate induced by BPA. Displacement refers to the pulling distance of the wire connected to both corners of the laminate. The Roman numerals in the load profile in (a) correspond to that of each snapshot in (b). (b) Snapshots of the CFRP laminate with a large curvature by BPA. (c) ABAQUS simulation of BPA.

(i) As the actuator pulls the tensile wire, the CFRP laminate edge flattens until the wire is almost straight. As the wire becomes straighter and tighter, the tensile force increases.

(ii) When the tensile force reaches the maximum load, the laminate edge bends in the other direction, and the force decreases and the laminate starts to deform.

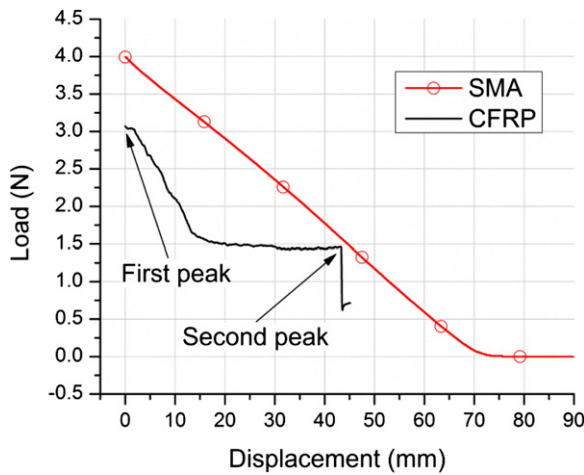


Figure 12. Actuation result of the SMA spring for BPA. The actuation result is over plotted on the load profile of the CFRP laminate by BPA. The displacement is the amount of reduced displacement between the two actuating points.

- (iii) The configuration of the laminate changes from a cylindrical shape to a saddle shape.
- (iv) The bending load decreases until half of the laminate surface has switched curvature sign.
- (v) After the bending deformation passes through the midpoint, the bending load maintains a constant value.
- (vi) When the original curvature of the laminate disappears, snap-through actuation occurs.
- (vii) After snap-through, the entire configuration of the laminate remains in the other stable shape.

5.2. Actuation test of SMA coil spring

To actuate the artificial leaf of the flytrap robot, the force generated by the SMA spring has to exceed the snap-through force of the laminate. Based on the load profile of the laminate and the stiffness of the sample SMA spring, the desired spring stiffness and stroke were calculated by simple linear fitting of two peaks of the load profile of the laminate (see figure 12). The first peak is when the laminate starts to deform and the second peak is when the snap-through occurs. The initial force of the desired SMA spring was set with a 10% safety margin from the maximum load of the laminate. The number of spring coils was determined by using the spring stiffness equation under the serially connected condition based on the sample SMA spring’s stiffness because the SMA spring in the austenite phase has a linear actuation like that of conventional mechanical springs. For the closing motion by the common unbending actuation, the same SMA spring actuator as that in the opening motion because the force for closing the leaf is smaller than that for opening the leaf.

To determine the appropriate actuation conditions of the SMA coil spring, the SMA spring actuation test was conducted using an electric current control. Before the test, the spring was treated four times with electric current heat training to saturate its load characteristic [31]. In the training setup, both ends of the spring were held by clamps of a tensile machine.

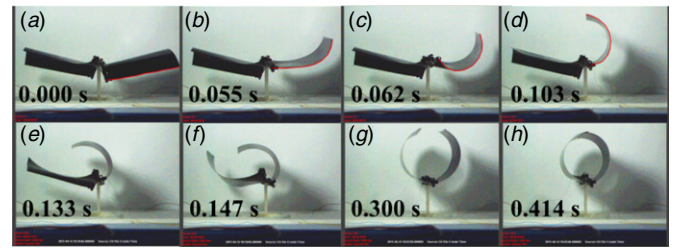


Figure 13. High-speed sequences of the closing motion. The recording rate was 1500 fps. The red line on the edge of the right CFRP leaf is the tracking line.

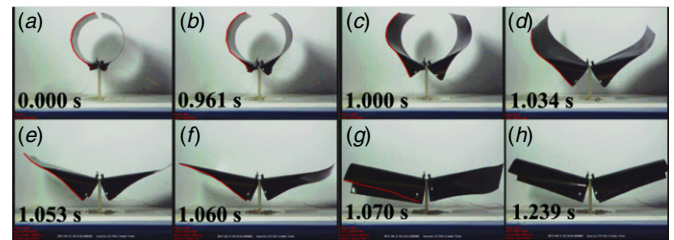


Figure 14. High-speed sequences of the opening motion. The recording rate was 1000 fps. The red line on the edge of the left CFRP leaf is the tracking line.

The spring was stretched by the tensile machine at room temperature. The electric current from a power supply went into the spring to change the martensitic phase to the austenitic phase. The current was held until the measured maximum force did not decrease over a period of 5 s in a single training cycle. The current was maintained constant, and the tensile machine slowly released the stretched SMA spring until the measured load reached zero. As determined during the heat training process, the appropriate test conditions of the sample SMA spring should be a maximum linear stroke of 1.25 mm/coil with an electric current of 0.6 A. When the applied current exceeded 0.6 A, the phase characteristics of the SMA spring changed owing to re-annealing by electrical overheating. In addition, although the current condition was satisfied, more than 1.25 mm tensile displacement in a spring coil caused thermomechanical yielding of the spring in the austenite phase.

5.3. Analysis of Rapid Locomotion of the flytrap robot

The snap-through sequences of the flytrap robot were recorded at 1,000 fps with a high-speed camera, as shown in figures 13 and 14. The actuation for the closing motion used 12.4 J over 4.5 s, and the actuation for the opening motion used 48 J over 10 s. The frequency of actuation between opening and closing depends on the sum of actuating time and cooling time of SMA spring. Usually in the flytrap robot, the SMA spring actuator is cooled down over 7.5 s. Thus, the operating frequency of the flytrap robot from closing to opening is about 0.046 Hz. Although the frequency of actuation is very low, most of the time was spent on triggering and cooling the actuation; the snap-through actuation took less than 0.1 s. The Venus flytrap also takes a long time to trigger its leaves but snaps very

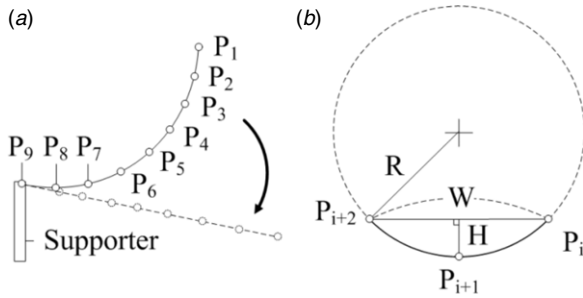


Figure 15. (a) Position of nine tracking points. (b) Schematic diagram of partial curvature calculation using three neighboring points.

quickly. Furthermore, we verify the natural frequency of the artificial leaf that has been measured to be 5.31 Hz at the closed state and 4.57 Hz at the open state. These measured frequencies close to frequencies calculated by numerical simulation that 7.77 Hz at the closed state and 2.43 Hz at the open state.

When we recorded the trapping motion of the robot, it was difficult to synchronize the closing times of both CFRP leaves simultaneously (see figure 13). The asymmetric actuation arose from fine errors of the SMA spring actuator during manual fabrication and embedding or from locally different stiffness of the CFRP laminate. Nevertheless, overall snapping occurred in about 0.4 s (the time included vibrations of the leaves), and it was difficult to discern the unsynchronized actuation of the robot with the naked eye.

To verify the deformation during opening by BPA, we used the motion analysis program ProAnalyst that traces coordinate data of nine points at the curve of the laminate in the side view (see figure 18(a)). Note that the intervals between the points were approximated by the naked eye, and we tried to keep the interval as consistent as possible.

As an indicator of the deformation, we chose the partial curvature of the curve through three serial points among the nine tracking points. The exact curvature of a general plane curve is presented in equation (6). However, in this case, the 3-point curve has a small slope (dy/dx) so that the contribution of the slope (dy/dx) in equation (6) is negligible. Thus, equation (6) can be reduced to equation (7), and the 3-point curve can be regarded as an arc of a circle. With this condition, we can calculate the curvature of the 3-point curve by using equation (8). To calculate the curvature using equation (8), the width and the height of the curve were required. The width was a chord length between the first and the third points, and the height was the distance between the second point and the chord (see figure 15(b)). The equation for the curvature of the 3-point curve is given below:

$$\kappa = \frac{\left| \frac{d^2y}{dx^2} \right|}{\left[1 + \left(\frac{dy}{dx} \right)^2 \right]^{3/2}} \quad (1)$$

$$\kappa = \left| \frac{d^2y}{dx^2} \right|, \quad \text{when } \left(\frac{dy}{dx} \right)^2 \ll 1 \quad (2)$$

$$\kappa = \frac{8H}{W^2 + 4H^2}, \quad (3)$$

where W is the width, H is the height and κ is curvature of the 3-point curve. Changes in seven partial curvatures are plotted in figures 16 and 17.

According to the trend of partial curvature changes in figures 16 and 17, the deformations during opening and closing were different depending on the actuation method. As shown in figure 16, BPA during opening changed the curved edge of the artificial leaf into a straight line. The snap-through action was initiated at point 8 and propagated to point 2 in sequence. The curvature of point 8 was initially almost zero because the unbending deformation rate at point 8 near the actuator was higher than the rate at the other points (see figures 14(a) and (b)); thus, points 7–9 formed a curve with negative curvature. The deformation by BPA propagated from the actuation point to the free end of the artificial leaf very well. Figure 17 shows the rapid curvature changes during closing of the CFRP leaf. In this case, the snap-through actuation induced the curvature change that started at point 2 the free end of the leaf and propagated to the point 8 the actuation point. Therefore, the artificial leaves could wrap rapidly and the flytrap robot could catch an object without missing.

5.4. Capturing performance and the CFRP pressing test

The actual flytrap can trap insects perfectly inside its leaves because it has a fanwise fiber orientation that allows the leaf to form an enclosed space when the leaf closes. Unlike the real flytrap, the bistable CFRP structure of the flytrap robot has a cylindrical shape since the fibers of CFRP are aligned unidirectionally. Since the CFRP is not produced with fanwise fiber orientation, the flytrap robot requires an additional part to cover the open section of the artificial leaf. When the artificial leaf closes, the side edge of the leaf becomes straight to curve. We utilize this shape transition to design the covering part, and improve the flytrap robot's leaf to provide an enclosed space as shown in figure 18. Pins are embedded at regular intervals on a surface near the straight edge of the artificial leaf, and thin acrylic sectors are attached on the pins. All centers of the sectors are upward when the leaf is open, while the centers meet the center of the curved edge when the leaf is closed. Therefore, acrylic sectors can build a large sector that covers the side open section of the leaf. By doing so, the flytrap robot can enclose the cavity, and it can capture objects like a baseball and a paper lizard.

As shown in figures 18(d) and (f), the flytrap robot can grip objects with various sizes. This gripping mechanism is simple and intuitive. An object larger than the cavity of the flytrap robot pushes out the CFRP leaf and the deformation of the CFRP leaf induces recovery force. This force works to grip the object, and it can be approximated by the gripping force. Therefore, the gripping force is determined passively by the object size. However, measuring the gripping force is difficult because it depends on the contact angle. In addition, applying force in a different direction by altering the deformation of the structure is difficult. For simplicity, we defined the gripping force as a normal force where the direction is normal to the line between two endpoints of the curve, as shown in figure 19(b). The assumption is that the laminate changes its shape with

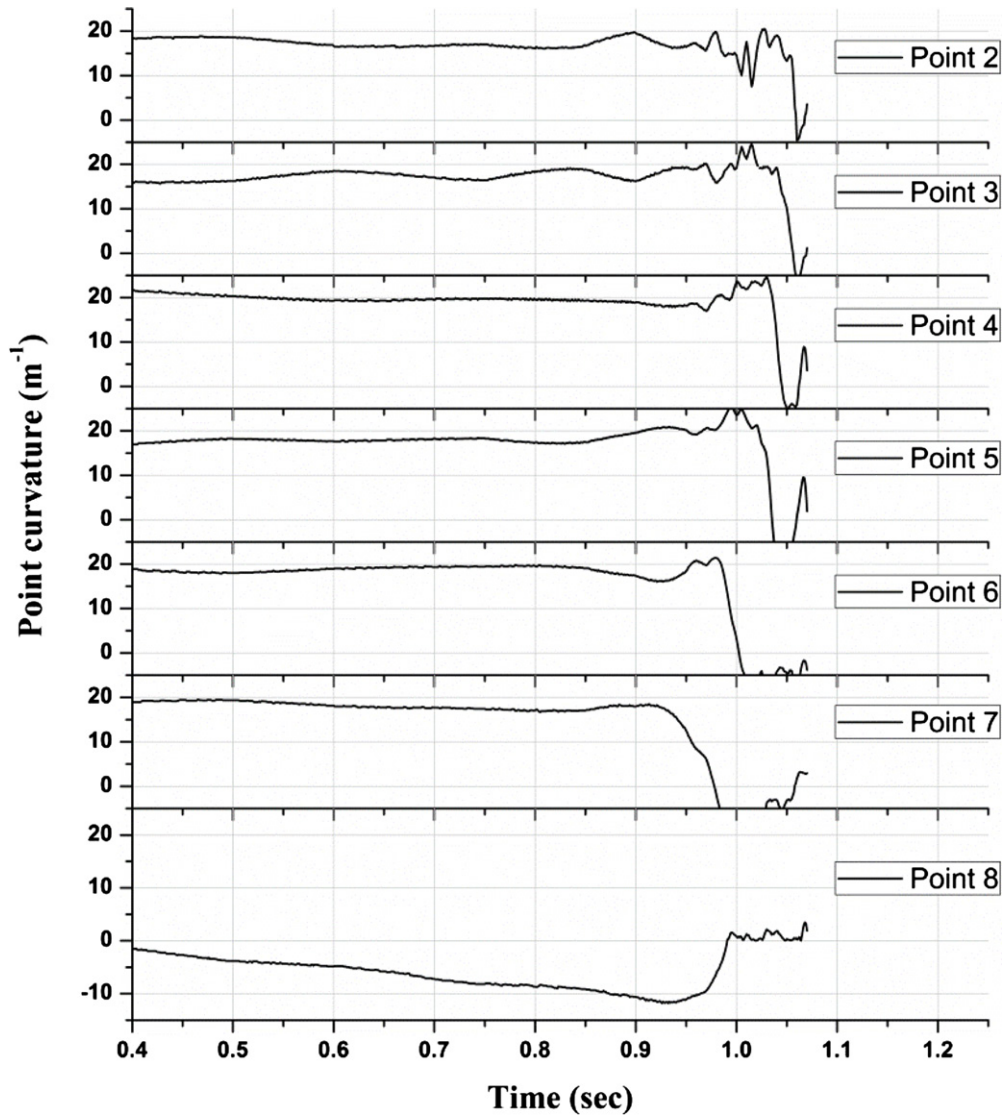


Figure 16. Partial curvature changes at each point on the edge of the CFRP leaf during opening.

constant curvature, which means that the deformed shape remains cylindrical. Although this concept is a rough approach to find the relation between the gripping force and the shape deformation, the measured force can be a reference for the gripping performance. In order to verify the relation, we set up the pressing test shown in figure 19(c). The tip block connected to the tensile machine pressed the center of the CFRP laminate with the tensile machine oriented vertically. As the laminate was pressed, its height reduced and its width increased. The mirror was used as a ground plate to minimize the friction.

The force–displacement graph is shown in figure 20(a): the upper line indicates the load to deform the initially large-curved shape, and the lower line indicates the load to deform the initially small-curved shape. The gripping force can be defined as the load required deforming the large curved laminate, which is the robot leaf in the closed state. Therefore, the profile of the upper line indicates the gripping force. When the large curved bistable CFRP was pressed, the curvature

reduced gradually (see figure 20(b) above). After a moment, the shape did not remain circular, and the middle part of the laminate became nearly flat. However, both edges remained as a curved shape (see figure 20(b) below). Owing to this nonlinear trajectory of the shape deformation, the load profile was nonlinear.

As shown in figure 20(a), the available weight of gripping was less than 50 g. As noted earlier, the gripping force is equal to the recovery force against the deformation of the laminate. The force is related to the bending stiffness of the laminate. The thickness of CFRP laminate was very thin, so its bending stiffness was very low. Thus, the current gripping force was insufficient to grip a heavy object. One way to increase the gripping force is by changing the properties of the CFRP laminate such as width, thickness and modulus. By assuming that the CFRP laminate keeps a cylindrical shape during deformation, we can treat this problem as a one-dimensional composite beam bending against pure moment. From one-dimensional composite beam bending theory, the

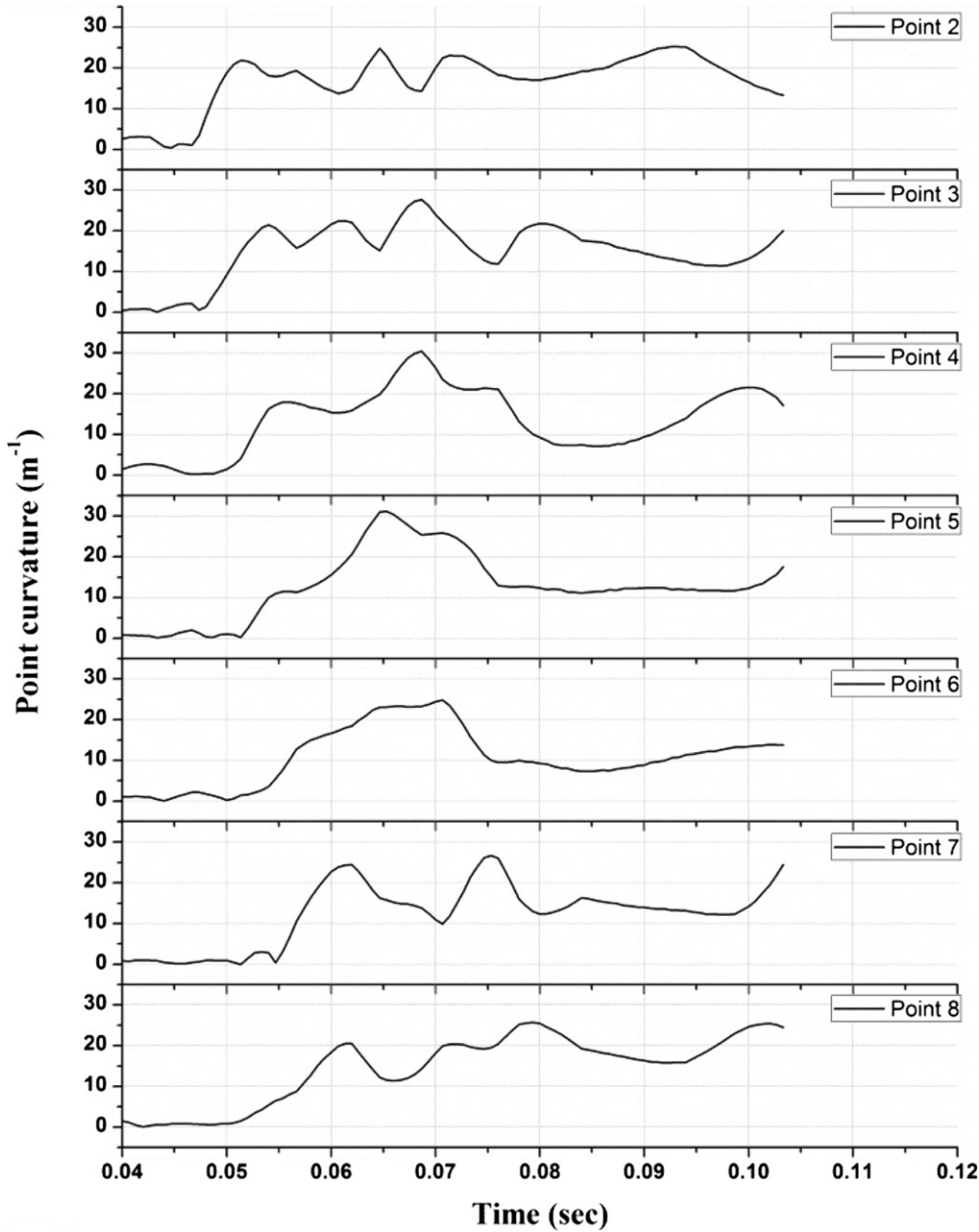


Figure 17. Partial curvature changes at each point on the edge of the CFRP leaf during closing.

relationship between the geometry and force/moment is given below:

$$E_1 \int_{A_1} z \, dA + E_2 \int_{A_2} z \, dA = 0 \tag{4}$$

$$\bar{z} = \frac{t}{4} \left(\frac{E_1 + 3E_2}{E_1 + E_2} \right) \tag{5}$$

$$I_i = \frac{1}{96} b t^3 + A_i (y_i - \bar{z})^2 \quad (i = 1, 2) \tag{6}$$

$$\begin{aligned} M &= \int_A \sigma_x z \, dA \\ &= \int_{A_1} \sigma_{x1} z \, dA + \int_{A_2} \sigma_{x2} z \, dA \end{aligned}$$

$$\begin{aligned} &= \kappa E_1 \int_{A_1} z^2 \, dA + \kappa E_2 \int_{A_2} z^2 \, dA \\ &= \kappa (E_1 I_1 + E_2 I_2) \end{aligned} \tag{7}$$

$$M = \frac{FL}{4} = \kappa (E_1 I_1 + E_2 I_2) \propto b t^3, \tag{8}$$

where E is modulus, A is area of the cross section of composite layer, \bar{z} is the height of neutral axis, t is thickness, b is width, I is moment inertia, M is bending moment, σ is normal stress on the cross section, κ is curvature induced by the bending moment, F is applied force and L is chord of the curve. According to equation (5), the bending moment is proportional to the width and the cube of the thickness. Therefore, increasing the thickness is an effective way to increase the gripping force.

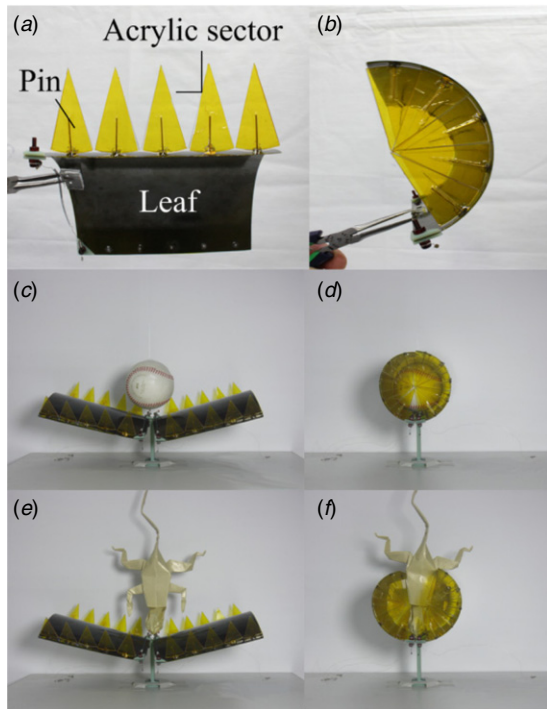


Figure 18. Side covering part of the flytrap robot’s leaf. When the leaf closes, each acrylic sector gets together and builds a large sector that covers the side open section of the flytrap robot’s leaf. By the side covering part, the flytrap robot can trap an object like a baseball and catch a paper lizard.

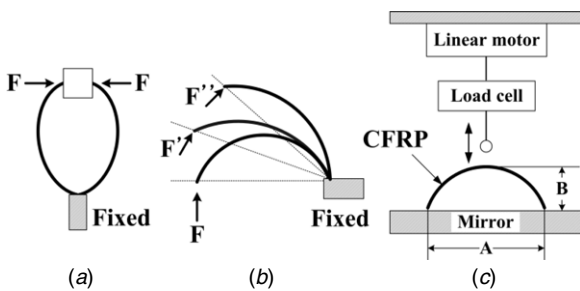


Figure 19. Schematic of concept of the flytrap robot gripping an object. (b) Illustration of deformation of CFRP leaf with applied force. (c) Schematic of the pressing CFRP laminate: A indicates the distance between two tip points of the CFRP laminate, and B indicates the height of the CFRP laminate.

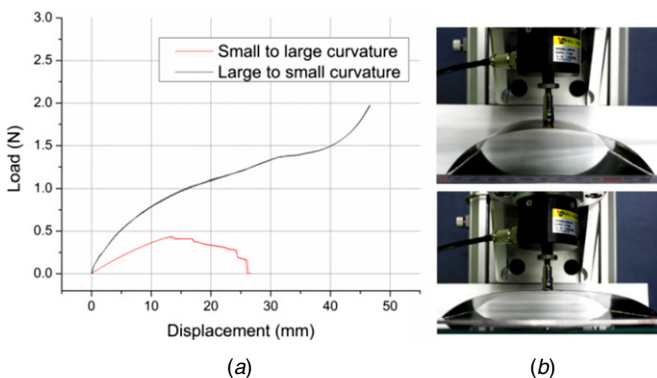


Figure 20. (a) Load profile of pressing the CFRP leaf. (b) The upper figure shows small deformation, and the lower figure shows large deformation.

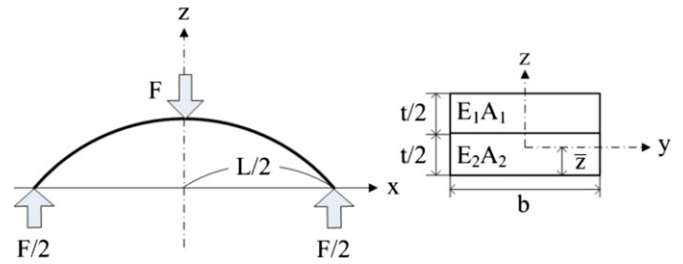


Figure 21. Schematic of bistable CFRP laminate showing geometry.

6. Conclusion

In this paper, we presented the flytrap robot and its structurally integrated actuation to generate a desired motion of soft body effectively and efficiently. The flytrap robot consists of bistable CFRP structures acting as the artificial leaf and SMA spring actuators. The structurally integrated actuation is based on a novel hardware design that uses the structural characteristics of the bistable CFRP structure: bistability and the characteristic of a developable surface. The bistability works as an implicit actuator, providing rapid closing motion, while not protruding from the device. This reduces the number of actuators and improves energy efficiency. Using bistability, the flytrap robot closes its leaf within 100 ms, which is the same as the Venus flytrap’s snapping time. The characteristic of a developable surface works as a kinematic constraint that reduces the number of DOF, providing a novel path for actuation. Using the developable surface characteristic and SMA coil spring actuators, BPA can create the desired large unbending motion of the artificial leaf even though the applied force direction of the SMA spring actuators is very different to that of the desired motion. The shape of the artificial leaf changes from semicircular in the closed state to flat in the open state and vice versa; the frequency of trapping is 0.046 Hz and curvature change is 18 m^{-1} .

The results of the flytrap robot demonstrate that utilizing bistability could be worthwhile in some designs for soft-bodied robots that create motion with large deformation. Bistability enables soft robots to have a simple structural design, two stable configurations in a single structure, and allows the creation of a rapid and large morphing motion by a simple actuation, regardless of the infinite DOF of the structure. This is applicable to morphing aircraft wings, where the wing shape would adjust depending on changes in the flight condition for efficient flight. In addition, it might be applied to a gripper on small-scale robots or biomedical devices enabling rapid and stable grasping of objects without continuous energy input.

In the current state of the flytrap robot, the bistable CFRP structure has a low gripping force. In addition, its shape depends on the thermomechanical properties; thus, its geometrical size and shape are limited, although we used novel manufacturing to change the curvature. Future work will involve parametric studies of the bistable structure to solve these problems. We plan to develop various kinds of bistable structures consisting of different materials, including CFRP, and different geometries, and we will test their structural characteristics. We expect that the results of the parametric

studies might provide a solution to these problems and be a reference for practical applications.

Acknowledgments

This research was supported by the Converging Research Center Program (2013K000371), Basic Science Research Program (2009-0087640), the Priority Research Centers Program (2012-041247), and the creative research program (2012R1A3A2048841, 2012-041247) through the National Research Foundation of Korea (NRF) funded by the Ministry of Science, ICT and Future Planning (MSIP), Republic of Korea.

References

- [1] Darwin C 1875 *Insectivorous Plants* (London: Murray)
- [2] Stuhlman O Jr 1948 Venus' fly-trap *Bull. Torrey Botanical Club* **75** 22–44
- [3] Hodick D and Sievers A 1989 On the mechanism of trap closure of Venus flytrap (*Dionaea muscipula* Ellis) *Planta* **179** 32–42
- [4] Forterre Y, Skotheim J M, Dumais J and Mahadevan L 2005 How the Venus flytrap snaps *Nature* **433** 421–5
- [5] Volkov A G, Adesina T, Markin V S and Jovanov E 2008 Kinetics and mechanism of *Dionaea muscipula* trap closing *Plant Physiol.* **146** 694–702
- [6] Yang R, Lenaghan S C, Zhang M and Xia L 2010 A mathematical model on the closing and opening mechanism for Venus flytrap *Plant Signal. Behav.* **5** 968–78
- [7] Kim S-W, Koh J-S, Cho M and Cho K-J 2010 Towards a bio-mimetic flytrap robot based on a snap-through mechanism *IEEE RAS and EMBS Int. Conf. on Biomedical Robotics Biomechatronics (BioRob)* pp 534–9
- [8] Kim S-W, Koh J-S, Cho M and Cho K-J 2011 Design and analysis a flytrap robot using bistable composite *IEEE Int. Conf. on Robotics and Automation* pp 215–20
- [9] Shahinpoor M 2011 Biomimetic robotic Venus flytrap (*Dionaea muscipula* Ellis) made with ionic polymer metal composites *Bioinspir. Biomim.* **6** 046004
- [10] Kim S-W, Koh J-S, Cho M and Cho K-J 2012 Soft morphing motion of flytrap robot using bending propagating actuation *J. Inst. Control, Robot. Syst.* **18** 168–74
- [11] Sciciliano B, Sciavicco L, Villani L and Oriolo G 2009 *Robotics: Modelling, Planning and Control* (Berlin: Springer) chapter 1
- [12] Steltz E, Mozeika A, Rembisz J, Corson N and Jaeger H M 2010 Jamming as an enabling technology for soft robotics *Proc. SPIE* **7642** 764225
- [13] Lin H T, Leisk G G and Trimmer B 2011 GoQBot: a caterpillar-inspired soft-bodied rolling robot *Bioinspir. Biomim.* **6** 026007
- [14] Sugiyama Y and Hirai S 2006 Crawling and jumping by a deformable robot *Int. J. Robot. Res.* **25** 603–20
- [15] Trivedi D, Rahn C D, Kier W M and Walker I D 2008 Soft robotics: biological inspiration, state of the art, and future research *Appl. Bionics Biomech.* **5** 99–117
- [16] Seok S, Onal C D, Cho K J, Wood R J, Rus D and Kim S 2013 Meshworm: a peristaltic soft robot with antagonistic nickel titanium coil actuators *IEEE/ASME Trans. Mech.* **18** 1485–97
- [17] Cianchetti M, Arienti A, Follador M, Mazzolai B, Dario P and Laschi C 2011 Design concept and validation of a robotic arm inspired by the octopus *Mater. Sci. Eng. C* **31** 1230–39
- [18] Mazzolai B, Margheri L, Cianchetti M, Dario P and Laschi C 2012 Soft-robotic arm inspired by the octopus: II. from artificial requirements to innovative technological solutions *Bioinspir. Biomim.* **7** 025006
- [19] Chang B C M, Berring J, Venkataram M, Menon C and Parameswaran M 2011 Bending fluidic actuator for smart structures *Smart Mater. Struct.* **20** 035012
- [20] Chang B C M, Chew A, Naghshineh N and Menon C 2012 A spatial bending fluidic actuator: fabrication and quasi-static characteristics *Smart Mater. Struct.* **21** 045008
- [21] Shepherd R F, Ilievski F, Choi W, Morin S A, Stokes A A, Mazzeo A D, Chen X, Wang M and Whitesides G M 2011 Multigait soft robot *Proc. Natl Acad. Sci. USA* **108** 20400–3
- [22] Martinez R V, Fish C R, Chen X and Whitesides G M 2012 Elastomeric origami: programmable paper-elastomer composites as pneumatic actuators *Adv. Func. Mater.* **22** 1376–84
- [23] Hufenbach W, Gude M and Czulak A 2006 Actor-initiated snap-through of unsymmetric composites with multiple deformation states *J. Mater. Process. Tech.* **175** 225–30
- [24] Mattioni F, Weaver P M, Potter K D and Friswell M I 2008 Analysis of thermally induced multistable composites *Int. J. Solids Struct.* **45** 657–75
- [25] Ryu J, Kong J-P, Kim S-W, Koh J-S, Cho K-J and Cho M 2013 Curvature tailoring of unsymmetric laminates with an initial curvature *J. Compos. Mater.* **47** 3163–74
- [26] Dano M L and Hyer M W 2003 SMA-induced snap-through of unsymmetric fiber-reinforced composite laminates *Int. J. Solids Struct.* **40** 5949–72
- [27] Schultz M R and Hyer M W 2003 Snap-through of unsymmetric cross-ply laminates using piezoceramic actuators *J. Intell. Mater. Syst. Struct.* **14** 795–814
- [28] Kim H A, Betts D N, Salo A I T and Bowen C R 2010 Shape memory alloy-piezoelectric active structures for reversible actuation of bistable composites *AIAA J.* **48** 1265–8
- [29] Gauss K F, Hildebeitel A and Morehead J 1902 *General Investigations of Curved Surfaces of 1827 and 1825* (Princeton: The Princeton University Library)
- [30] An S-M, Ryu J, Cho M and Cho K-J 2012 Engineering design framework for a shape memory alloy coil spring actuator using a static two-state model *Smart Mater. Struct.* **21** 055009
- [31] Otsuka K and Wayman C M 1998 *Shape Memory Materials* (Cambridge: Cambridge University Press) chapter 11 pp 240–3
- [32] Noh M, Kim S-W, An S-M, Koh J-S and Cho K-J 2012 Flea-inspired capapult mechanism for miniature jumping robots *IEEE Trans. Robot.* **28** 1007–18
- [33] Follador M, Cianchetti M, Arienti A and Laschi C 2012 A general method for the design and fabrication of shape memory alloy active spring actuators *Smart Mater. Struct.* **21** 115029